Journal of Solar Energy Research (JSER)

Journal homepage: www.jser.ut.ac.ir

Analysis of Intrastring Line-to-Line Fault in Photovoltaic System

Hamid Reza Parsa[a], Mohammad Sarvi[b]

[a] *Faculty of Technical and Engineering, Imam Khomeini International University, Qazvin, Iran.*
[b] *School of Electrical Engineering, Iran University of Science and Technology, Tehran, Iran.*

ARTICLE INFO

Article Type:

Research Article

Received:22.10.2023
Accepted:27.05.2024

Keywords:
Line-line fault
P-V curve
Extreme points
MPPT controller
Photovoltaic

A B S T R A C T

Line-to-line fault (LLF) is one of the most important fault occurring in photovoltaic (PV) systems. necessitating comprehensive investigation and analysis to develop optimal fault detection methodologies. This study focuses on analyzing a specific LLF variant known as intrastring line-to-line fault (ISLLF), wherein one or more modules within individual strings are short-circuited. The power-voltage (P-V) and current-voltage (I-V) curves of PV systems contain extensive data valuable for fault detection. Thus, exact analysis of these curves to extract various features is essential. The extremum points of P-V curve indicate the severity of occurred faults in PV system. In this paper, different states of triple and quadruple ISLLF are simulated and according to the obtained result, mathematical equations are presented for extremum values. Additionally, the performance of the maximum power point tracking (MPPT) controller is evaluated, and the requisite constraints for optimal power selection using MPPT across different states of the P-V curves are presented. The derived equations suggest insights into accurately determining the severity and location of LLF occurrences.

1. Introduction

Nowdays, the generation of electrical energy using solar systems is very important. Therefore, it is necessary to identify and diagnose possible faults in these systems in order to increase the stability and reliability.

Yong et al. presented an effective method for partial shading (PS) recognition and fault severity diagnosis in photovoltaic (PV) arrays. The proposed diagnosing of PS fault. The data preparation phase composes of pre-processing and conversion procedures for I-V curves, ensuring a reliable data source for subsequent analysis [1]. [2] developed a data-driven technique with high repeatability for extracting I-V curve parameters and distributed this method as an open-source package. This technique is able to characterize the large volumes of PV module I–V data. Mingyao Ma et al. investigated the I-V curve of various faulty modules and proposed a

*Corresponding Author Email:msarvi@iust.ac.ir

Cite this article: Parsa, H. R., & Sarvi, M. (2024). Analysis of Intra-String Line-Line Fault in Photovoltaic System. Journal of Solar Energy Research, 9(1), 1780-1793. doi: 10.22059/jser.2024.367117.1352

DOI: 10.22059/jser.2024.367117.1352

new method for diagnosing different faults based on obtained data. Also, the exponential function was used to amplify the fault characteristic value [3]. A fuzzy logic based on MPPT method was employed in that used the PV curves. In this method, a new parameter was applied to increase the MPPT precision [4]. Authors in [5] evaluate the PV panel performance using I-V polynomial function. The obtained model has an applicable performance in tracking the maximum power points in partial shading condition. [6] proposed a new method for tracking the global peak (GP) in power-voltage (P-V) curves of PV systems. This method can be applied in uniform irradiance and PS conditions. The method tracks all the local points and selects the maximum power point among them as GP. Different MPPT algorithms were reviewed in [7] and the authors investigated the advantages and disadvantages of each method in different conditions and also introduced appropriate ones. [8] proposed a MPPT algorithm with high accuracy in PS conditions. The experimental results confirmed the good performance of this method compared to perturb and observe (P&O) algorithm. Huang et al. designed a novel method for diagnosing different faults in PV systems based on I-V curve. Also, fault features are optimized and then extracted by analyzing the I-V curves in faulty conditions [9]. [10] proposed a new intelligent method for detecting and diagnosing different faults in PV arrays. This method used a new deep network model with extracting features from I-V curves in different irradiation levels and ambient temperatures. Authors in [11] proposed a numerical approach in order to create a function for I-V curve fitting. For this purpose, the least square algorithm was used for determining the equation parameters and also the Newton– Raphson method was applied for solving the obtained equations. The fitted model has low deviation in comparison with measured data.

A novel method was proposed in order to extract five key parameters of PV module including series and shunt resistances, photo current, reverse saturation current density, and diode ideal factor. In this method, five equations were presented considering the relation between the I-V curves and aforementioned parameters. In [12], the measured data validated the equations in different irradiation levels and temperatures. Gude and Jana used a technique called cuckoo search optimization (CSO) and also modified (MCSO) and improved (ICSO) type of this method in order to extract the PV cell parameters. The obtained results from these algorithms were compared with experimental data [13]. Qais et al. presented a new PV model considering three-diode circuit. For this purpose, the coyote optimization algorithm (COA) was applied for extracting some parameters of PV module. This algorithm considered the root mean square (RMS) current error between the calculated and experimental values [14]. In other literature, two algorithms such as Rao-2 (R-II), and Rao-3 (R-III) were used in order to estimate the required parameters of PV module. The experimental results validated the accuracy of the proposed methods in comparison with statistical ones [15]. Also [16] discussed a new algorithm namely hybridized interior search (HIS) in order to estimate the essential parameters of PV module. To assess the algorithm performance, RMSE has been used as an index for comparison between the calculated and empirical values. The proposed method has been validated by comparing the one with other methods. [17] approximated the unknown parameters of PV module using a new optimizer namely sine cosine algorithm (SCA). Also, this algorithm has been improved by the opposition-based learning scheme and the Nelder-Mead simplex. Qais et al. exploited the sunflower optimization (SFO) in order to design PV parameters. To assess the proposed algorithm, the validation of I-V and P-V curves was performed with measured data in different weather conditions [18]. Authors suggested a fast and accurate method namely MADE for estimation of PV parameters. This method used the success-history and the Nelder-Mead simplex for the global and local searches, respectively [19]. A comparative study on parameter extraction of PV module has been presented in [20]. For this purpose, eleven differential evolution (DE) algorithms are compared to achieve the accurate PV models. [21] applied the slime mould algorithm (SMA) as a new method for estimation of PV parameters. This method is able to treat the non-linearity of PV curves. Also, this method has been compared comprehensively with present methods and the results demonstrated the accuracy performance of the proposed approach. In order to predict the performance of PV system, modeling of the I-V curve for PV module is important. The authors in [22] combined the Lambert-W function and an iterative process. The proposed method achieved good results for experimental I-V curves obtained in various irradiation levels and temperatures. Zhicong Chen et al. proposed a new black-box modeling approach for PV modules. They used one-dimensional deep residual network (1-D ResNet) and the measured I-V curves as the train data. Also, the datasets of I-V

curves in partial shading condition were considered in this method. A comprehensive comparison has been presented between the proposed method and other artificial neural network algorithms in order to validate the accuracy and reliability of 1-D ResNet [23]. In order to obtain an accurate model of PV module, an improved Lozi map based chaotic optimization algorithm (ILCOA) was proposed [24]. This algorithm estimates the critical parameters of PV panels. The proposed method has a good performance in comparison with other similar algorithms. In other study, a differential evolution algorithm was proposed for estimation of PV model parameters. This algorithm is based on self-adaptive ensemble. To assess the proposed algorithm, it was applied for three PV models and the results validated its capability [25]. Hao et al. suggested a new approach in order to identify the PV module parameters in different operating points of PV curves. Also, an objective function was applied for reaching to optimum parameters. For this purpose, five critical points of I-V curves were considered [26].

A two-step method was suggested by authors in [27] for designing an accurate model of PV array. In the first step, they extracted the model parameters and obtained the MPP of P-V curve in the second step. Then, random forest classifiers (RFC) were used in the fault detection process.

A new simple method was proposed for detecting and diagnosing the faulty states for grid-connected PV system. The rate of variation of currant and voltage trajectory in I-V curve was considered in this method. The proposed approach is able to detect different faulty cases and also determine the severity of them [28].

An artificial neural network (ANN) was used in order to detect and diagnose different types of faults in PV system. The input data is including irradiation levels and ambient temperatures and also the voltage and current values at GMP in healthy conditions were considered as targets. Moreover, a second ANN was designed for fault classification [29].

Authors in [30] proposed two algorithms for PV fault detection and identification. The first algorithm presented a method for thresholding and the second one is designed based on fuzzy logic classification. Li et al. suggested a sensorless approach for detecting different faults in PV system. This method also exploits the inflection point of I-V curve in order to distinguish PS conditions precisely. Also, the proposed method is efficient in fault localization and determining the mismatch level [31]. Finally, an intelligent method was proposed for diagnosing the PV faults. This method utilizes the I-V curves and also variable predictive models. In this method, the I-V curves were investigated in various operating conditions at STC and key points have been extracted from these curves. The mentioned points were used as input data of proposed algorithm after normalization [32].

In this paper, two types of LLF in different states are investigated. For this purpose, the impact of these faults on P-V curves are discussed. In order to evaluate these curves, mathematical equations are presented for maximum and minimum points. Theses equation can be applied for different sizes of PV arrays. The results of this study are used for detecting of faulty strings and determining the number of short-circuited module precisely.

Section 2 analyzes the P-V curve of triple ISLLF and presents the mathematical equations for extremum points. The other type of ISLLF, namely quadruple is investigated in section 3. The analysis of results and discussion are provided in section 4. Finally, the conclusions are presented in section 5.

2. Triple Intrastring Line-to-Line Fault

To show the severity of LLF in different states, an index called mismatch level is defined as following

$$ML = \frac{f}{m} \times 100 \quad (1)$$

where m, and f are the number of modules in each string, and the number of short-circuited modules in the faulty strings, respectively.

This section analysis triple ISLLF. It means three or more strings with three different mismatch values have been short circuited in the PV array. So, in order to demonstrate the different states of this fault, four samples are considered. For this purpose, simulation of the PV system is performed in MATLAB for healthy and different cases of LLF. The PV array is composed of eight modules connected in series (m=8) in five parallel strings (n=5) as illustrated in Figure 1. As can be seen, the blocking diodes have been embedded for each strings. These diodes prevent negative currents from passing through the strings. The selected modules for simulation are Solartech Energy ASC-6M-72C-325-3BB model. The PV module specifications at standard test conditions (STC) are given in Table 1. In STC, the cell temperature and the irradiation level are 25 (℃) and 1000 (W/m^2), respectively.

The P-V curves can be used as an important criterion in evaluating different conditions of the PV systems

in healthy and faulty states. Figure 2 shows the P-V curve of healthy (fault-free) condition at STC.

As shown, this curve has only a global maximum at 13 (KW). Also, at global maximum power point (GMP), the array voltage (V_a) and the array current (I_a) are 309.3 (V) and 42.04 (Amp), respectively. Also, V_a is equal to is 8 times module voltage at GMP (V_m), and I_a is 5 times module current at GMP (I_m).

In the first sample, four modules from the first string (50% mismatch), six modules from the second string (75% mismatch), and two modules from the third string (25% mismatch) have been short circuited and the other strings are healthy. The P-V curve has seven extrema as illustrated in Figure 3. As can be seen, the extremum points include four maxima and three minima. The current, voltage, and power values for PV array at extremum points are presented in Table 2.

As shown, the array voltage at maximum points is approximated as coefficient V_m. Also, the array current at these points is written approximately as a linear combination of I_m and short-circuit current of module (I_{sc}). The array current and voltage values at minimum points are correction coefficients of I_{sc} and open-circuit voltage of module (V_{oc}), respectively. So, the voltage values of extremum points can be used for determining the number of short-circuited modules in each faulty strings.

The PV system is analyzed in four maxima as

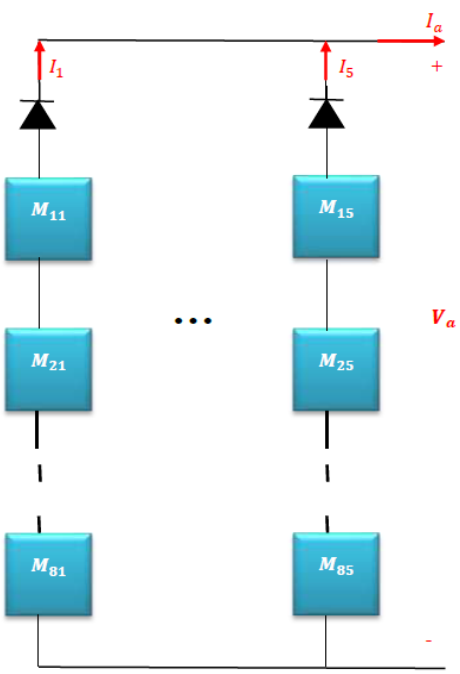

Figure 1. The schematic of PV array

Table 1. PV module specifications at STC

Parameter	Value
Maximum power (P_m)	325 W
Open-circuit voltage (V_{oc})	46.6 V
Short-circuit current (I_{sc})	9.0 A
Voltage at MPP (V_m)	38.7 V
Current at MPP (I_m)	8.4 A

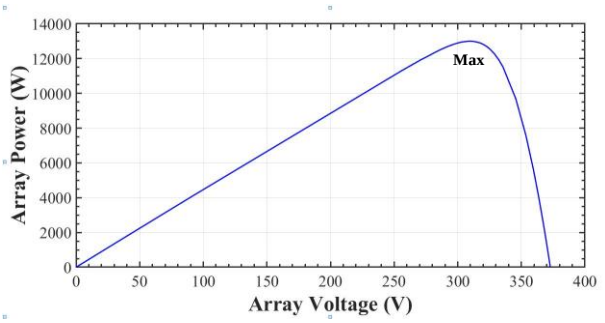

Figure 2. The P-V curve of healthy condition at STC

operating points. For this purpose, the voltage to current ratio of the array at each operating point is considered as a resistance load for the PV system and then the voltage and current values of modules are obtained. In order to justify the state of the array at any maximum point, the string currents for these points are given in Table 3. The array voltage at maximum points is proportional to the number of healthy modules in the mentioned faulty strings.

In the first maximum, the current values of all strings are non-zero. As can be seen, the maximum current flows along the fourth and fifth (healthy) strings and the minimum current passes the second string (75% mismatch). Consequently, as the severity of the fault in each string increases, the current value of faulty strings decreases.

In the second maximum, the current of the second string (75% mismatch) is zero, i.e., the faulty string is considered as out of the PV system. The values of the modules in this state are the same as when an open circuit fault occurred in this string, but these two types of faults can be differentiated. There are three differences between these two faulty states. The differences are related to the P-V curve, the array short circuit current, and the voltage of blocking diode in the faulty string. The array short circuit of PV system is equal to 45 (Amp), but this value is 36 (Amp) in open circuit fault. This value decreased according to number of open-circuited strings. In this operating point, the absolute voltage value across the blocking diode in the second string is 72.2 (V) but this value is zero when this string is open circuited.

In the third maximum, the currents of two faulty strings are zero and the currents in the fourth and fifth strings are almost equal to I_{sc}.

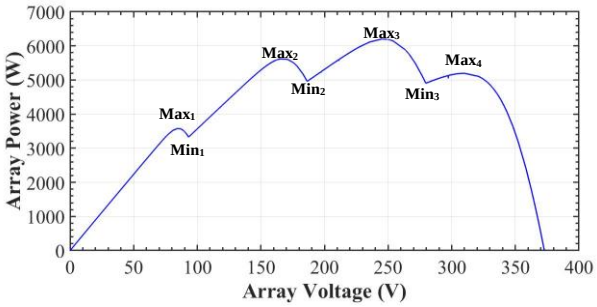

Figure 3. The P-V curve of the first sample at STC

In the fourth maximum, all of the currents in faulty strings are zero. Also, the voltage and current values of healthy modules are V_m and I_m, respectively. So, the array power is equal to 40% of one in healthy state.

According to the I-V curve of the PV module in STC, the voltage of healthy modules in each string is obtained for the first sample at all operating points as given in Table 4. Also, the absolute voltage values across the blocking diodes at maximum points are presented for this sample in Table 5.

By applying the maximum power point tracking (MPPT) controller and considering the power values in Table 2, the third maximum (Max_3) is selected as GMP.

In the second sample, three modules from the first string (37.5% mismatch), seven modules from the third string (87.5% mismatch), and five modules from the fifth string (62.5% mismatch) have been short circuited. The P-V curve consists of four maximums and three minimums as shown in Figure 4. The extremum values of PV array are given in Table 6. As can be seen, the current, voltage and power values at the fourth maximum *(max_4)* remain constant in comparison with Table 2.

When the MPPT controller is applied, the fourth maximum is selected as GMP. In this point, the current of all faulty strings are zero. So, the currents flowing the healthy strings are equal to half of array current. In other words, the MPPT controller ignores all of the faulty strings in order to select the GMP. Since the LLF in the first sample is more severe than one in the second sample, the third maximum value in the first sample is higher than the same value in the second sample.

In the third sample, three modules from the first and third strings (37.5% mismatch), two modules from the second string (25% mismatch), and five modules from the fifth string (62.5% mismatch) have been short circuited. In this sample, the fault severity of the first and third strings are same, so this sample is considered as triple LLF. In other words, the mismatch values of faulty strings should be three distinct numbers.

Figure 5 shows the P-V curve of the third sample. It is observed that the second maximum *(max_2)* is selected as GMP by MPPT controller. When the PV array is operated at GMP as an operating point, the string currents are obtained as 7.911 (Amp), 8.812 (Amp), 7.911 (Amp), 8.879 (Amp), and 0 (Amp), respectively. As a result, the fifth string is ignored in process of finding the GMP. The extremum values of this sample are given in Table 7.

In this sample, the comparison of maximum values is expressed as

$$P_{\max_4} < P_{\max_3} < P_{\max_1} < P_{\max_2} \quad (2)$$

Table 2. Extremum values of P-V curve for the first sample at STC

Points	V_a (V)	I_a (Amp)	P_a (W)
Max_1	$84.49 \cong 2V_m$	$42.34 \cong I_m + 4I_{sc}$	$3577 \cong 2V_m \times (I_m + 4I_{sc})$
Min_1	$93.2 = 2V_{oc}$	$35.69 \cong 4I_{sc}$	$3328 \cong 8V_{oc} I_{sc}$
Max_2	$165.4 \cong 4V_m$	$33.97 \cong I_m + 3I_{sc}$	$5618 \cong 4V_m \times (I_m + 3I_{sc})$
Min_2	$186.4 = 4V_{oc}$	$26.61 \cong 3I_{sc}$	$4960 \cong 12V_{oc} I_{sc}$
Max_3	$246.4 \cong 6V_m$	$25.18 \cong I_m + 2I_{sc}$	$6204 \cong 6V_m \times (I_m + 2I_{sc})$
Min_3	$279.6 = 6V_{oc}$	$17.54 \cong 2I_{sc}$	$4904 \cong 12V_{oc} I_{sc}$
Max_4	$310 \cong 8V_m$	$16.78 \cong 2I_m$	$5197 \cong 16V_m I_m$

Table 3. The string currents for four operating points in the first sample

Points	I_1 (A)	I_2 (A)	I_3 (A)	I_4 (A)	I_5 (A)
Max_1	8.90	6.61	8.93	8.95	8.95

Max_2	7.30	0	8.87	8.90	8.90
Max_3	0	0	7.48	8.85	8.85
Max_4	0	0	0	8.39	8.39

The above inequality is different for the first and second samples. It means that the mismatch values of faulty strings determine the sort of power values at maximum points.

In the fourth sample, one module from the first and second strings (12.5% mismatch), four modules from the third and fourth strings (50% mismatch),

Table 4. Voltage values of healthy modules at maximum points in the first sample

Points	The first string	The second string	The third string	The fourth string	The fifth string
Max_1	21.12	42.25	14.08	10.56	10.56
Max_2	41.36	46.6	27.57	20.68	20.68
Max_3	46.6	46.6	41.07	30.8	30.8
Max_4	46.4	46.4	46.4	38.75	38.75

Table 5. Absolute voltage values across the blocking diodes at maximum points in the first sample

Points	The first string	The second string	The third string	The fourth string	The fifth string
Max_1	0	0	0	0	0
Max_2	0	72.22	0	0	0
Max_3	60.01	15.32	0	0	0
Max_4	123.6	216.8	30.38	0	0

and three modules from the fifth string (37.5% mismatch) have been short circuited. In this special case, all strings are faulty in triple ISLLF, but the P-V curve has three maxima and two minima as shown in Figure 6. In this state, the open circuit voltage of the array (326.2 V) is less than one (372.8 V) in the previous cases. This value is calculated as following:

$$V_{oc_a} = (m - f_3)V_{oc} \quad (3)$$

where f_3 is the least number of faulty modules among faulty strings. The power values at the first, second, and third maximums are 6836 (W), 5172 (W) and 4545 (W), respectively as given in Table 8.

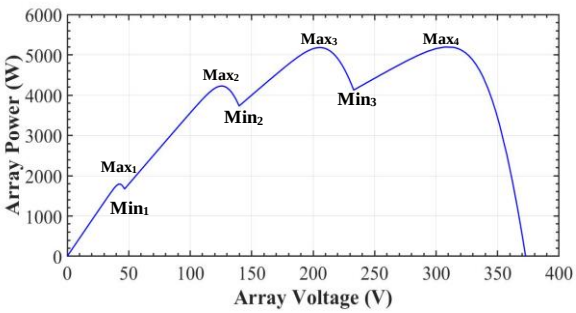

Figure 4. The P-V curve of the second sample at STC

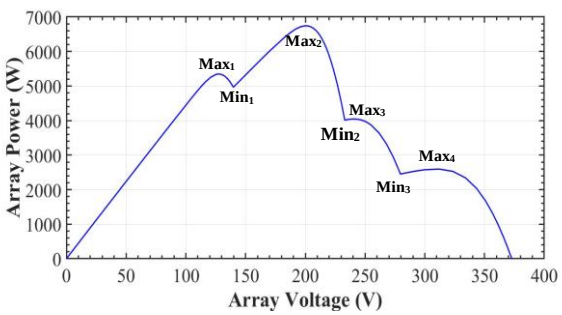

Figure 5. P-V curve of the third sample at STC

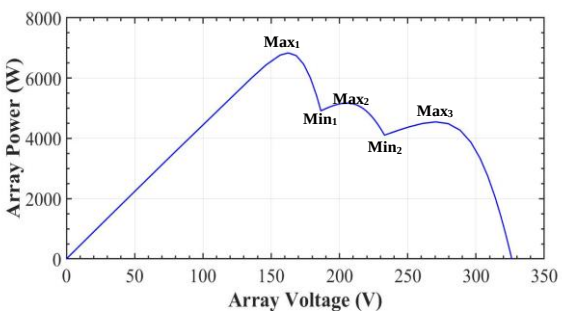

Figure 6. P-V curve of the fourth sample at STC

Table 6. Extremum values of P-V curve for the second sample at STC

Points	V (V)	I (A)	P (W)
Max_1	$43.16 \cong V_m$	$41.52 \cong I_m + 4I_{sc}$	$1792 \cong V_m \times (I_m + 4I_{sc})$
Min_1	$46.6 = V_{oc}$	$35.84 \cong 4I_{sc}$	$1670 \cong 4V_{oc}I_{sc}$
Max_2	$125.7 \cong 3V_m$	$33.62 \cong I_m + 3I_{sc}$	$4226 \cong 3V_m \times (I_m + 3I_{sc})$
Min_2	$139.8 = 3V_{oc}$	$26.69 \cong 3I_{sc}$	$3731 \cong 9V_{oc}I_{sc}$
Max_3	$206.2 \cong 5V_m$	$25.12 \cong I_m + 2I_{sc}$	$5179 \cong 5V_m \times (I_m + 2I_{sc})$
Min_3	$233 = 5V_{oc}$	$17.70 \cong 2I_{sc}$	$4125 \cong 10V_{oc}I_{sc}$
Max_4	$307.2 \cong 8V_m$	$16.91 \cong 2I_m$	$5195 \cong 16V_mI_m$

Table 7. Extremum values of P-V curve for the third sample at STC

Points	V_a (V)	I_a (Amp)	P_a (W)
Max_1	$128 \cong 3V_m$	$41.77 \cong I_m + 4I_{sc}$	$5347 \cong 3V_m \times (I_m + 4I_{sc})$
Min_1	$139.8 = 3V_{oc}$	$35.53 \cong 4I_{sc}$	$4967 \cong 12V_{oc}I_{sc}$
Max_2	$201.2 \cong 5V_m$	$33.51 \cong 2I_m + 2I_{sc}$	$6742 \cong 5V_m \times (2I_m + 2I_{sc})$
Min_2	$233 = 5V_{oc}$	$17.22 \cong 2I_{sc}$	$4012 \cong 10V_{oc}I_{sc}$
Max_3	$241.2 \cong 6V_m$	$16.77 \cong I_m + I_{sc}$	$4045 \cong 6V_m \times (I_m + I_{sc})$
Min_3	$279.6 = 6V_{oc}$	$8.77 \cong I_{sc}$	$2452 \cong 6V_{oc}I_{sc}$
Max_4	$312.1 \cong 8V_m$	$8.32 \cong I_m$	$2596 \cong 8V_mI_m$

Table 8. Extremum values of P-V curve for the fourth sample at STC

Points	V_a (V)	I_a (Amp)	P_a (W)
Max_1	$162.1 \cong 4V_m$	$42.17 \cong 2I_m + 3I_{sc}$	$6836 \cong 4V_m \times (2I_m + 3I_{sc})$
Min_1	$186.4 = 4V_{oc}$	$26.36 \cong 3I_{sc}$	$4914 \cong 12V_{oc}I_{sc}$
Max_2	$205 \cong 5V_m$	$25.23 \cong I_m + 2I_{sc}$	$5172 \cong 5V_m \times (I_m + 2I_{sc})$
Min_2	$233 = 5V_{oc}$	$17.62 \cong 2I_{sc}$	$4106 \cong 10V_{oc}I_{sc}$
Max_3	$273 \cong 7V_m$	$16.65 \cong 2I_m$	$4545 \cong 14V_mI_m$

3. Quadruple Intrastring Line-Line Fault

In the Quadruple ISLLF, the mismatch values of faulty strings should be four distinct numbers. The fifth sample is considered as this type of fault. In this sample, five, four, three and two modules from the first, second, third and fourth strings have been short circuited, respectively and the other string is healthy. The P-V characteristic of this state is illustrated in Figure 7. This curve consists of five maxima and four minima as given in Table 9. As can be seen, the number of maximum and minimum points increases by one unit compared with the triple ISLLF. the statues of PV system in five maxima as operating points are investigated as following. In the first maximum, the string currents are non-zero. When the PV system is operated in this point, the minimum current flows along the first string and the other string currents are almost equal to I_{sc}. When the second maximum is selected as the operating point, the current in string-1 is zero. Also, the current through the second string is approximately equal to I_m and the current values of three other strings are almost to I_{sc}. In other words, the MPPT controller selects the second maximum as GMP by ignoring the first string. Also, in the third operating point, the string currents in the first and second strings are equal to zero. A current approximately equal to I_m passes through the third string and I_{sc} flows the fourth and fifth strings.

In the fourth maximum, the current magnitude in three strings with the highest number of short-circuited modules, namely the first, second, and

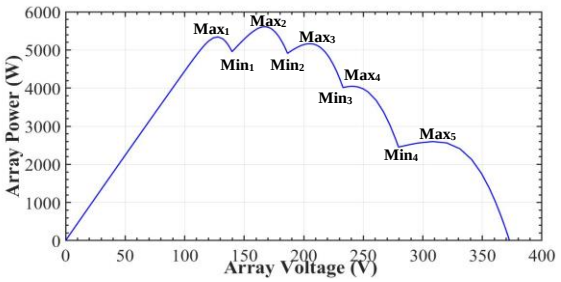

Figure 7. The P-V curve of the fifth sample at STC

third strings are zero and the currents of other strings are nearly equal to I_m and I_{sc}, respectively. In the last operating point, the current I_m passes the fifth string and the other string currents are zero.

The voltage of healthy modules and also the absolute voltage values across the blocking diodes in each string are obtained for five samples at GMP as given in Tables 10-11.

Table 9. Extremum values of P-V curve for the fifth sample at STC

Points	**V (V)**	**I (A)**	**P (W)**
Max_1	$128.1 \cong 3V_m$	$41.70 \cong I_m + 4I_{sc}$	$5341 \cong 3V_m \times (I_m + 4I_{sc})$
Min_1	$139.8 = 3V_{oc}$	$35.44 \cong 4I_{sc}$	$4954 \cong 12V_{oc}I_{sc}$
Max_2	$167 \cong 4V_m$	$33.58 \cong I_m + 3I_{sc}$	$5609 \cong 4V_m \times (I_m + 3I_{sc})$
Min_2	$186.4 = 4V_{oc}$	$26.35 \cong 3I_{sc}$	$4911 \cong 12V_{oc}I_{sc}$
Max_3	$205 \cong 5V_m$	$25.19 \cong I_m + 2I_{sc}$	$5164 \cong 5V_m \times (I_m + 2I_{sc})$
Min_3	$233 = 5V_{oc}$	$17.22 \cong 2I_{sc}$	$4012 \cong 10V_{oc}I_{sc}$
Max_4	$240.9 \cong 6V_m$	$16.79 \cong I_m + I_{sc}$	$4045 \cong 6V_m \times (I_m + I_{sc})$
Min_4	$279.6 = 6V_{oc}$	$8.77 \cong I_{sc}$	$2452 \cong 6V_{oc}I_{sc}$

Table 10. Voltage values of healthy modules for five samples at GMP

Points	The first sample	The second sample	The third sample	The fourth sample	The fifth sample
V_h^1	21.12	46.6	40.25	23.16	46.6
V_h^2	42.25	38.41	33.54	23.16	41.76
V_h^3	14.08	46.6	40.25	40.52	33.41
V_h^4	10.56	38.41	25.15	40.52	27.84
V_h^5	10.56	46.6	46.6	32.42	20.88

Table 11. Absolute voltage values across the blocking diodes for five samples at GMP

Points	The first sample	The second sample	The third sample	The fourth sample	The fifth sample
V_D^1	60.01	74.31	0	0	27.25
V_D^2	15.32	0	0	0	0
V_D^3	0	260.7	0	0	0
V_D^4	0	0	0	0	0
V_D^5	0	167.5	61.43	0	0

4. The proposed algorithm

According to the obtained results in previous sections, one of the maximum points depending on the mismatch values in faulty strings is selected as GMP. As shown in previous sections, the MPPT

controller selects the third, fourth, second, first and second local maxima for five samples as GMP, respectively. To investigate the MPPT controller performance for determining the GMP, some parameters are defined for triple ISLLF as follows:
The mismatch index (N_i) is defined for each faulty string with the mismatch value, f_i as:

$$N_i = \frac{A_i}{B_i}, \qquad \text{for } i = 1,2,3 \tag{4}$$

The numerator of this index (A_i) for each mismatch value is expressed as:

$$A_1 = m \times \left[\left(2k_1 + k_2 + k_3 - n\right) I_m + (n - k_1) I_{sc} \right] \tag{5}$$

$$A_2 = m \times \left[\left(2k_2 + k_1 + k_3 - n\right) I_m + (n - k_1 - k_2) I_{sc} \right] \tag{6}$$

$$A_3 = m \times \left[\left(2k_3 + k_1 + k_2 - n\right) I_m + (n - k_1 - k_2 - k_3) I_{sc} \right] \tag{7}$$

where k_1, k_2, and k_3 are the number of faulty strings with the number of f_1, f_2 and f_3 short circuited

modules respectively.
Also, the dominator of N_i (B_i) for each mismatch value is defined as

$$B_1 = k_1 I_m + (n - k_1) I_{sc} \tag{8}$$

$$B_2 = k_2 I_m + (n - k_1 - k_2) I_{sc} \tag{9}$$

$$B_3 = k_3 I_m + (n - k_1 - k_2 - k_3) I_{sc} \tag{10}$$

where B_1, B_2, and B_3 are defined accordance to f_1, f_2, and f_3, respectively.
It can be shown that the following inequality is always true.

$$N_3 < N_2 < N_1 \tag{11}$$

According to defined indexes, the process of sorting the local maxima in order to select the GMP by MPPT controller is expressed as follows.
Firstly, in order to compare the fourth maximum power with other maximum points, below constraints are investigated as follows:

$$\text{If } f_i \geq N_i \Rightarrow P_{\max_i} \leq P_{\max_4} \quad \text{for } i=1,2,3. \tag{12}$$

$$\text{If } f_i \leq N_i \Rightarrow P_{\max_i} \geq P_{\max_4} \quad \text{for } i=1,2,3. \tag{13}$$

Secondly, in order to determine the most value among the first, second, and third maxima, the relative mismatch value index called f_{ij} is defined between two faulty strings with different number of faulty modules f_i and f_j as follows:

$$f_{ij} = \frac{B_i f_i - B_j f_j}{B_i - B_j} \geq m \Rightarrow P_{\max_i} \leq P_{\max_j} \ ,$$

$$f_{ij} = \frac{B_i f_i - B_j f_j}{B_i - B_j} \leq m \Rightarrow P_{\max_i} \geq P_{\max_j}$$

$$i<j, \quad \textit{for } i, j=1,2,3. \tag{14}$$

According to the simulation results in the previous sections, mathematical equations for extremum points are generalized as following. For this purpose, it is assumed f_1, f_2, f_3, …, and f_p modules in different strings have been short circuited by the number of k_1, k_2, …, and k_p strings, respectively. Extremum points of the P-V curve are obtained assuming below constraints as given in Table 12.

$$1 \leq f_p < f_{p-1} < \ldots < f_2 < f_1 \leq m \tag{15}$$

$$k_1 + k_2 + \ldots + k_p \leq n \tag{16}$$

Also, the mismatch index in its general form is defined as:

$$N_j = \frac{A_j}{B_j}, \qquad \textit{for } j=1, 2, \ldots, p. \tag{17}$$

Generally, the equations (5)-(10) are rewritten for $j=1,2,\ldots,p$ as:

$$A_j = m \times \left[\left(k_j - n + \sum_{i=1}^{p} k_i \right) \times I_m + \left(n - \sum_{i=1}^{j} k_i \right) \times I_{sc} \right] \tag{18}$$

$$B_j = k_j \times I_m + \left(n - \sum_{i=1}^{j} k_i \right) \times I_{sc} \tag{19}$$

where k_j is the number of strings with f_j faulty modules.
To compare the last maximum power with other maximum points, below constraints are checked for $i=1,2,\ldots,p$ as follows:

$$\text{If } f_i \leq N_i \Rightarrow P_{\max_i} \geq P_{\max_{p+1}} \tag{20}$$

If $f_i \geq N_i \Rightarrow P_{\max_i} \leq P_{\max_{p+1}}$ (21)

To identify the maximum value among the maximum points under the assumption ($i<j$, $i,j=1,2,3,\ldots,p$), the following constraints are investigated as

$$f_{ij} = \frac{B_i f_i - B_j f_j}{B_i - B_j} \geq m \Rightarrow P_{\max_i} \leq P_{\max_j} \quad (22)$$

$$f_{ij} = \frac{B_i f_i - B_j f_j}{B_i - B_j} \leq m \Rightarrow P_{\max_i} \geq P_{\max_j} \quad (23)$$

Also, the number of faulty modules ($N^i{}_f$) in i^{th} string can be expressed as:

$$N^i{}_f = m - \frac{V_a - V_D^i}{V_h^i} \quad (24)$$

where V_D^i and V_h^i are the absolute value of the voltage across the blocking diode and the voltage of healthy modules in the i^{th} string, respectively.
The above equation can accurately determine the number of faulty modules for each maximum (operating) point.

5. Validation of Results and Discussion

To validate the proposed algorithm, the obtained results for the first, third and fifth samples are investigated. For this purpose, the required parameters for comparison the maximum points are provided in Table 13.
In the first sample, given that $f_1 > N_1$, $f_2 < N_2$, and $f_3 < N_3$, so, according to equations (12)-(13), the inequalities are expressed as follows:

$$P_{\max_2} \geq P_{\max_4}, \quad P_{\max_3} \geq P_{\max_4}, \quad P_{\max_1} \leq P_{\max_4} \quad (25)$$

Also, f_{12}, f_{13}, and f_{23} are more than the number of modules in each string (m=8), according to equation (14), the below inequalities are written as:

$$P_{\max_1} \leq P_{\max_2}, \quad P_{\max_1} \leq P_{\max_3}, \quad P_{\max_2} \leq P_{\max_3} \quad (26)$$

The combination of equations (25) and (26) is written as

$$P_{\max_1} \leq P_{\max_4} \leq P_{\max_2} \leq P_{\max_3} \quad (27)$$

Table 12. Extremum values of P-V curve for ISLLF (general form)

Points	V (V)	I (A)	P (W)
Max_1	$(m-f_1)V_m$	$k_1 I_m + (n-k_1) I_{sc}$	$(m-f_1)V_m \times [k_1 I_m + (n-k_1) I_{sc}]$
Min_1	$(m-f_1)V_{oc}$	$(n-k_1) I_{sc}$	$(m-f_1)(n-k_1) V_{oc} I_{sc}$
. . .	. . .	. . .	. . .
Max_h	$(m-f_h)V_m$	$k_h I_m + \left(n - \sum_{i=1}^{h} k_i\right) I_{sc}$	$(m-f_h)V_m \times \left[k_h I_m + \left(n - \sum_{i=1}^{h} k_i\right) I_{sc}\right]$
Min_h	$(m-f_h)V_{oc}$	$\left(n - \sum_{i=1}^{h} k_i\right) I_{sc}$	$(m-f_h)\left(n - \sum_{i=1}^{h} k_i\right) V_{oc} I_{sc}$
. . .	. . .	. . .	. . .
Max_P	$(m-f_p)V_m$	$k_p I_m + \left(n - \sum_{i=1}^{p} k_i\right) I_{sc}$	$(m-f_p)V_m \times \left[k_p I_m + \left(n - \sum_{i=1}^{p} k_i\right) I_{sc}\right]$
Min_P	$(m-f_p)V_{oc}$	$\left(n - \sum_{i=1}^{p} k_i\right) I_{sc}$	$(m-f_p)\left(n - \sum_{i=1}^{p} k_i\right) V_{oc} I_{sc}$
Max_{P+1}	mV_m	$\left(n - \sum_{i=1}^{p} k_i\right) I_m$	$mV_m \times \left(n - \sum_{i=1}^{p} k_i\right) I_m$

The values of Figure 3 and Table 2 confirm the validity of equation (27).
In the third sample, since $f_1 < N_1$, $f_2 < N_2$, and $f_3 < N_3$ so according to equations (20)-(21), the inequalities are written as

$$P_{max_2} \geq P_{max_4}, \quad P_{max_3} \geq P_{max_4}, \quad P_{max_1} \geq P_{max_4} \tag{28}$$

According to equations (22) and (23), each of the parameters f_{12}, f_{13} and f_{23} is compared to the number of modules in each string (m=8). So, the comparison leads to the following inequalities

$$P_{max_1} \leq P_{max_2}, \quad P_{max_3} \leq P_{max_1}, \quad P_{max_3} \leq P_{max_2} \tag{29}$$

The following inequality is obtained from the combination of (28) and (29)

$$P_{max_4} \leq P_{max_3} \leq P_{max_1} \leq P_{max_2} \tag{30}$$

The values of Figure 5 and Table 7 confirm the equation (30) and the MPPT controller selects the second maximum as GMP.
In the fifth sample, since $f_1 < N_1$, $f_2 < N_2$, $f_3 < N_3$, and $f_4 < N_4$, so, the following inequalities are expressed based on equations (20) and (21).

Table 13. Required parameters for comparison the maximum points

Parameters	The first sample	The third sample	The fifth sample
A_1	220.8	288.0	288.0
A_2	148.8	211.2	216.0
A_3	76.8	72.0	144.0
A_4	-	-	72.0
B_1	44.4	44.4	44.4
B_2	35.4	34.8	35.4
B_3	26.4	17.4	26.4
B_4	-	-	17.4
N_1	4.97	6.49	6.49
N_2	4.20	6.07	6.10
N_3	2.91	4.14	5.45
N_4	-	-	4.14
f_{12}	13.87	12.25	8.93
f_{13}	11.87	6.93	7.93
f_{23}	9.87	4.00	6.93
f_{14}	-	-	6.93
f_{24}	-	-	5.93
f_{34}	-	-	4.93

$$P_{max_1} \geq P_{max_3}, \qquad P_{max_2} \geq P_{max_5},$$

$$P_{max_4} \geq P_{max_5} \qquad P_{max_3} \geq P_{max_5}, \tag{31}$$

According to equations (22) and (23), each of the parameters f_{12}, f_{13}, f_{14}, f_{23}, f_{24} and f_{34} is compared to the number of modules in each string (m=8). Therefore, Consequently, the comparison yields the following inequalities:

$$P_{max_2} \geq P_{max_1}, \quad P_{max_1} \geq P_{max_3}, \quad P_{max_1} \geq P_{max_4},$$

$$P_{max_2} \geq P_{max_3}, \quad P_{max_2} \geq P_{max_4}, \quad P_{max_3} \geq P_{max_4} \tag{32}$$

The following inequality is derived from the combination of equations (31) and (32).

$$P_{max_5} \leq P_{max_4} \leq P_{max_3} \leq P_{max_1} \leq P_{max_2} \tag{33}$$

The data presented in Figure 7 and Table 9 corroborate equation (33).
Also, in order to validate equation (24), the number of faulty modules for the first sample at four maximum points were calculated as given in Table 14. For this purpose, the results of Tables 4-5 were used. Furthermore, Table 15 presents the number of short circuited modules for five samples at GMP using the data of Tables 10-11. The results demonstrate the effectiveness of the suggested formula in identifying the number of faulty modules. For additional confirmation, the obtained results were compared with previous ones in other literatures. It is worth mentioning that only a few studies have addressed the performance of PV curves in details. The authors in [33] presented several approximate formulas to evaluate the performance of the MPPT controller. They considered line-line faulty conditions with low severity, while our method provides exact equations for all extrema points of the P-V curve and comprehensively interprets this curve under various faulty conditions.

6. Conclusions

This paper investigated different types of ISLLF such as triple and quadruple faults. The P-V curve of PV system for different mismatch values have been analyzed. The mathematical equations were obtained for extremum points and then the MPPT performance in order to select the maximum power

was evaluated based on definition some indexes. Finally, the general state of ISLLF was considered and then general formulas have been presented using simulation results. In order to validate the proposed equations, three samples were investigated and also the performance of MPPT controller were presented in selecting the MPP. The results demonstrated the accuracy of mathematical equations and defined indexes. The obtained equations are useful for determining the severity and location of LLF. Although, the simulation of PV system was performed at STC, but the obtained mathematical equations can be used for different module temperatures and irradiation levels. For future work, the aforementioned equations can be obtained for various states of partial shading faults.

Table 14. Number of faulty modules in each string at different operating points in the first sample

Points	The first string	The second string	The third string	The fourth string	The fifth string
Max_1	3.999	6.001	1.999	-0.00095	-0.00095
Max_2	4.001	6.000	2.001	0.0023	0.0023
Max_3	4.000	6.000	2.001	0.0003	0.0003
Max_4	4.000	6.000	1.999	0.0002	0.0002

Table 15. Number of faulty modules in each string at GMP

Points	The first string	The second string	The third string	The fourth string	The fifth string
The first sample	4.000	6.000	2.001	0.0003	0.0003
The second sample	3.002	0.002	7.002	0.0021	5.002
The third sample	3.001	2.001	3.001	0.0003	5.001
The fourth sample	1.001	1.001	3.999	3.999	3.001
The fifth sample	5.001	4.001	3.002	2.002	0.0023

Nomenclature	
ANN	Artificial neural network
COA	Coyote optimization algorithm
CSO	Cuckoo search optimization
DE	Differential evolution
f_i	Number of faulty modules in each faulty strings
GMP	Global maximum power point (W)
GP	Global peak (W)
HIS	Hybridized interior search
LLF	Line-to-line fault
I_a	Array current (Amp)
I_m	current at MPP (Amp)
I_{sc}	Short-circuit current of module (Amp)
ILCOA	Improved Lozi map based chaotic optimization algorithm
ISLLF	Intra-string line-to-line fault
I-V	Current-Voltage
m	Number of modules in each string
MPP	Maximum power point (W)
MPPT	Maximum power point tracking
n	Number of strings in PV array
N_i	Mismatch index
N^i_f	Number of faulty modules
P_a	Array voltage
PCA	Principal component analysis
P_{max_1}	Power value at the first maximum (W)
P_{max_2}	Power value at the second maximum (W)
P_{max_3}	Power value at the third maximum (W)
P_{max_4}	Power value at the fourth maximum (W)
P_{max_5}	Power value at the second maximum (W)
PS	Partial shading
PV	Photovoltaic
P-V	Power-Voltage
P&O	Perturb and Observe
RFC	Random forest classifiers
RMS	Root mean square
RMSE	Root mean squared error
SCA	Sine cosine algorithm
SFO	Sunflower optimization
SMA	Slime mould algorithm
STC	Standard test conditions
V_a	Array voltage (V)
V_D^i	Absolute value of the voltage across the blocking diode in the i^{th} string (V)
V_m	Voltage at MPP (V)
V_{oc}	Open-circuit voltage of the module (V)
V_{oc_a}	Open-circuit voltage of the array (V)

References

[1] Yang, H., Ding, K., Chen, X., Jiang, M., Yang, Z., Zhang, J., & Gao, R. (2024). Fast simulation modeling and multiple-PS fault diagnosis of the PV array based on I–V curve conversion. *Energy Conversion and Management*, *300*, 117965. DOI: 10.1016/j.enconman.2023.117965.

[2] Ma, X., Huang, W. H., Schnabel, E., Köhl, M., Brynjarsdóttir, J., Braid, J. L., & French, R. H. (2019). Data-driven I-V feature extraction for photovoltaic modules. *IEEE Journal of Photovoltaics*, *9*(5), 1405-1412. DOI: 10.1109/JPHOTOV.2019.2928477.

[3] Ma, M., Zhang, Z., Yun, P., Xie, Z., Wang, H., & Ma, W. (2021). Photovoltaic module current mismatch fault diagnosis based on I-V data. *IEEE Journal of Photovoltaics*, *11*(3), 779-788. DOI: 10.1109/JPHOTOV.2021.3059425.

[4] Pandey, A. K., Singh, V., & Jain, S. (2023). Maximum power point tracking algorithm based on fuzzy logic control using PV and IV characteristics for PV array. *IEEE Transactions on Industry Applications*. DOI: 10.1109/TIA.2023.3272536.

[5] Mehta, H. K., & Panchal, A. K. (2021). PV panel performance evaluation via accurate V–I polynomial with efficient computation. *IEEE Journal of Photovoltaics*, *11*(6), 1519-1527. DOI: 10.1109/JPHOTOV.2021.3115250.

[6] Aquib, M., Jain, S., & Gosh, S. (2022). A Technique for Tracking the Global Peak of PV Arrays During Partially Shaded Conditions Using the Detection of Current Source and Voltage Source Regions of I–V Curves. *IEEE Journal of Emerging and Selected Topics in Industrial Electronics*, *3*(4), 1096-1105. DOI: 10.1109/JESTIE.2022.3150257.

[7] Sarvi, M., & Azadian, A. (2022). A comprehensive review and classified comparison of MPPT algorithms in PV systems. *Energy Systems*, *13*(2), 281-320. DOI: 10.1007/s12667-021-00427-x.

[8] Haj Seyed Aboutorabi, S. M., & Sarvi, M. (2020). A new method for solar array maximum power point determining and tracking. *Tabriz Journal of Electrical Engineering*, *49*(4), 1559-1567. https://sid.ir/paper/401772/en.

[9] Huang, J. M., Wai, R. J., & Gao, W. (2019). Newly-designed fault diagnostic method for solar photovoltaic generation system based on IV-curve measurement. *IEEE Access*, *7*, 70919-70932. DOI: 10.1109/ACCESS.2019.2919337.

[10] Chen, Z., Chen, Y., Wu, L., Cheng, S., & Lin, P. (2019). Deep residual network based fault detection and diagnosis of photovoltaic arrays using current-voltage curves and ambient conditions. *Energy Conversion and Management*, *198*, 111793. DOI: 10.1016/j.enconman.2019.111793.

[11] Abdulrazzaq, A. K., Bognár, G., & Plesz, B. (2022). Accurate method for PV solar cells and modules parameters extraction using I–V curves. *Journal of King Saud University-Engineering Sciences*, *34*(1), 46-56. DOI: org/10.1016/j.jksues.2020.07.008.

[12] Wei, D., Wei, M., Cai, H., Zhang, X., & Chen, L. (2020). Parameters extraction method of PV model based on key points of IV curve. *Energy conversion and management*, *209*, 112656. DOI: 10.1016/j.enconman.2020.112656.

[13] Gude, S., & Jana, K. C. (2020). Parameter extraction of photovoltaic cell using an improved cuckoo search optimization. *Solar Energy*, *204*, 280-293. DOI: 10.1016/j.solener.2020.04.036.

[14] Qais, M. H., Hasanien, H. M., Alghuwainem, S., & Nouh, A. S. (2019). Coyote optimization algorithm for parameters extraction of three-diode photovoltaic models of photovoltaic modules. *Energy*, *187*, 116001. DOI: 10.1016/j.energy.2019.116001.

[15] Premkumar, M., Babu, T. S., Umashankar, S., & Sowmya, R. (2020). A new metaphor-less algorithms for the photovoltaic cell parameter estimation. *Optik*, *208*, 164559. DOI: 10.1016/j.ijleo.2020.164559.

[16] Kler, D., Goswami, Y., Rana, K. P. S., &Kumar, V. (2019). A novel approach to parameter estimation of photovoltaic systems using hybridized optimizer. *Energy Conversion and Management*, *187*, 486-511. DOI: 10.1016/j.enconman.2019.01.102.

[17] Chen, H., Jiao, S., Heidari, A. A., Wang, M., Chen, X., & Zhao, X. (2019). An opposition-based sine cosine approach with local search for parameter estimation of photovoltaic models. *Energy Conversion and Management*, *195*, 927-942. DOI: 10.1016/j.enconman.2019.05.057.

[18] Qais, M. H., Hasanien, H. M., & Alghuwainem, S. (2019). Identification of electrical parameters for three-diode photovoltaic model using analytical and sunflower optimization algorithm. *Applied Energy*, *250*, 109-117. DOI: 10.1016/j.apenergy.2019.05.013.

[19] Li, S., Gong, W., Yan, X., Hu, C., Bai, D., & Wang, L. (2019). Parameter estimation of photovoltaic models with memetic adaptive differential evolution. *Solar Energy*, *190*, 465-474. DOI: 10.1016/j.solener.2019.08.022.

[20] Yang, X., Gong, W., & Wang, L. (2019). Comparative study on parameter extraction of photovoltaic models via differential evolution. *Energy conversion and management*, *201*, 112113. DOI: 10.1016/j.enconman.2019.112113.

[21] Mostafa, M., Rezk, H., Aly, M., & Ahmed, E. M. (2020). A new strategy based on slime mould algorithm to extract the optimal model parameters of solar PV panel. *Sustainable Energy Technologies and Assessments*, *42*, 100849. DOI: 10.1016/j.seta.2020.100849.

[22] Polo, J., Martín-Chivelet, N., Alonso-García, M. C., Zitouni, H., Alonso-Abella, M., Sanz-Saiz, C., & Vela-Barrionuevo, N. (2019). Modeling IV curves of photovoltaic modules at indoor and outdoor conditions by using the Lambert function. *Energy conversion and management*, *195*, 1004-1011. DOI: 10.1016/j.enconman.2019.05.085.

[23] Chen, Z., Chen, Y., Wu, L., Cheng, S., Lin, P., & You, L. (2019). Accurate modeling of photovoltaic modules using a 1-D deep residual network based on IV characteristics. *Energy conversion and management*, *186*, 168-187. DOI: 10.1016/j.enconman.2019.02.032.

[24] Pourmousa, N., Ebrahimi, S. M., Malekzadeh, M., & Alizadeh, M. (2019). Parameter estimation of photovoltaic cells using improved Lozi map based chaotic optimization Algorithm. *Solar Energy*, *180*, 180-191. DOI: 10.1016/j.solener.2019.01.026.

[25] Liang, J., Qiao, K., Yu, K., Ge, S., Qu, B., Xu, R., & Li, K. (2020). Parameters estimation of solar photovoltaic models via a self-adaptive ensemble-based differential evolution. *Solar Energy*, *207*, 336-346. DOI: 10.1016/j.solener.2020.06.100.

[26] Hao, P., Zhang, Y., Lu, H., & Lang, Z. (2021). A novel method for parameter identification and performance estimation of PV module under varying operating conditions. *Energy Conversion and Management*, *247*, 114689. DOI: 10.1016/j.enconman.2021.114689.

[27] Amiri, A. F., Oudira, H., Chouder, A., & Kichou, S. (2024). Faults detection and diagnosis of PV systems based on machine learning approach using random forest classifier. *Energy Conversion and Management*, *301*, 118076. DOI: 10.1016/j.enconman.2024.118076.

[28] Abd el-Ghany, H. A., ELGebaly, A. E., & Taha, I. B. (2021). A new monitoring technique for fault detection and classification in PV systems based on rate of change of voltage-current trajectory. *International Journal of Electrical Power & Energy Systems*, *133*, 107248. DOI: 10.1016/j.ijepes.2021.107248.

[29] Aallouche, A., & Ouadi, H. (2022). Online fault detection and identification for an isolated PV system using ANN. *IFAC-PapersOnLine*, *55*(12), 468-475. DOI: 10.1016/j.ifacol.2022.07.356.

[30] Bacha, M., & Terki, A. (2022). Diagnosis algorithm and detection faults based on fuzzy logic for PV panel. *Materials Today: Proceedings*, *51*, 2131-2138. DOI:10.1016/j.matpr.2021.12.490.

[31] Li, C., Yang, Y., Zhang, K., Zhu, C., & Wei, H. (2021). A fast MPPT-based anomaly detection and accurate fault diagnosis technique for PV arrays. *Energy Conversion and Management*, *234*, 113950. DOI: 10.1016/j.enconman.2021.113950.

[32] Liu, Y., Ding, K., Zhang, J., Lin, Y., Yang, Z., Chen, X., ... & Chen, X. (2022). Intelligent fault diagnosis of photovoltaic array based on variable predictive models and I–V curves. *Solar Energy*, *237*, 340-351. DOI: 10.1016/j.solener.2022.03.062.

[33] Miao, W., Lam, K. H., & Pong, P. W. (2020). A string-current behavior and current sensing-based technique for line–line fault detection in photovoltaic systems. *IEEE Transactions on Magnetics*, *57*(2), 1-6.